Journal of Medicinal Chemistry

Article

pubs.acs.org/jmc

# Investigating the Role of $T_7$ and $T_{12}$ Residues on the Biological Properties of Thrombin-Binding Aptamer: Enhancement of Anticoagulant Activity by a Single Nucleobase Modification

Nicola Borbone,[†] Mariarosaria Bucci,[‡] Giorgia Oliviero,[†] Elena Morelli,[#] Jussara Amato,[†] Valentina D'Atri,[†] Stefano D'Errico,[†] Valentina Vellecco,[‡] Giuseppe Cirino,[‡] Gennaro Piccialli,[†] Caterina Fattorusso,*[,†] Michela Varra,*[,†] Luciano Mayol,[†] Marco Persico,[†,§] and Maria Scuotto[†,§]

[†]Dipartimento di Chimica delle Sostanze Naturali, [‡]Dipartimento di Farmacologia Sperimentale, [#]Dipartimento di Chimica Farmaceutica e Tossicologica, Università degli Studi di Napoli Federico II, Via D. Montesano 49, 80131 Napoli, Italy

Supporting Information

**ABSTRACT:** An acyclic pyrimidine analogue, containing a five-member cycle fused on the pyrimidine ring, was synthesized and introduced at position 7 or 12 of the 15-mer oligodeoxynucleotide GGTTGGTGTGGTTGG, known as thrombin-binding aptamer (TBA). Characterization by $^1$H NMR and CD spectroscopies of the resulting aptamers, TBA-$T_7$**b** and TBA-$T_{12}$**b**, showed their ability to fold into the typical antiparallel chairlike G-quadruplex structure formed by TBA. The apparent CD melting temperatures indicated that the introduction of the acyclic residue, mainly at position 7, improves the thermal stability of resulting G-quadruplexes with respect to TBA. The anticoagulant activity of the new molecules was then valued in PT assay, and it resulted that TBA-$T_7$**b** is more potent than TBA in prolonging clotting time. On the other hand, in purified fibrinogen assay the thrombin inhibitory activity of both modified sequences was lower than that of TBA using human enzyme, whereas the potency trend was again reversed using bovine enzyme. Obtained structure−activity relationships were investigated by structural and computational studies. Taken together, these results reveal the active role of TBA residues $T_7$ and $T_{12}$ and the relevance of some amino acids located in the anion binding exosite I of the protein in aptamer−thrombin interaction.

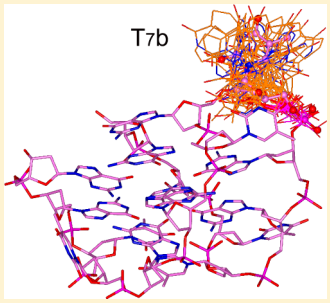


## INTRODUCTION

Thrombin is a sodium-activated allosteric enzyme playing a key role in blood coagulation.[1a,b] The complexity of thrombin function and regulation has gained this enzyme pre-eminence as the prototypic allosteric serine protease.[2a−e] It clots blood by converting fibrinogen into fibrin, by activating factors V, VIII, and XIII, the latter being responsible for the cross-linking of fibrin fibers, and by promoting platelet aggregation. Because activation of factor V is required by activated factor X to cut prothrombin into thrombin, the synthesis of thrombin is in part modulated by its own blood concentration, thus providing a fast response to injury. Besides procoagulant stimuli, also anticoagulant stimuli can be triggered by thrombin via activation of protein C, under the allosteric control of the cofactor thrombomodulin. Moreover, thrombin inactivation and clearance in plasma can also be achieved by interaction with the serpin antithrombin and with the heparin cofactor II. Due to its central role in the coagulation cascade, malfunctions in the regulatory mechanism of thrombin activity cause pathological states such as hemorrhage or abnormal clot growth. Thrombosis and connected diseases are among the main causes of mortality in Western countries;[3] thus, the discovery of molecules capable of modulating thrombin activity represents a major target for the development of anticoagulant strategies.[4] Aptamer technology has been efficiently employed to obtain new direct thrombin inhibitors by selecting thrombin-binding oligonucleotides.[5] The term aptamer generally refers to a single-stranded oligonucleotide that binds to a selected protein and specifically inhibits one or more of its functions. The first reported consensus sequence able to inhibit thrombin activity was the 15-mer oligonucleotide (ON) GGTTGGTGTGGTTGG, usually known with the acronym TBA (thrombin-binding aptamer).[5a] In the presence of thrombin and/or monovalent cations TBA folds into a specific three-dimensional structure that dictates its thrombin-binding affinity. The structures of TBA alone and in complex with thrombin were determined by NMR[6] and X-ray[7] methods, respectively. In all experimentally determined structures TBA adopted a monomolecular chairlike G-quadruplex folding topology, consisting of two G-tetrads connected by one TGT loop and two TT loops. First,[7a,b] different TBA−thrombin X-ray complexes were reported, in which TBA adopted either the same folding as derived by NMR (PDB ID 1HAO; Figure 1A) or a different one (PDB IDs 1HUT and 1HAP; Figure 1B), presenting a diverse positioning of the connecting loops.

In these X-ray complexes, the aptamer interacts with distinct regions of two thrombin molecules, (i) the fibrinogen exosite (namely anion-binding exosite I, ABE I) and (ii) the heparin exosite (namely, ABE II) near the carboxylate terminal helix of

**Received:** September 28, 2012
**Published:** November 5, 2012

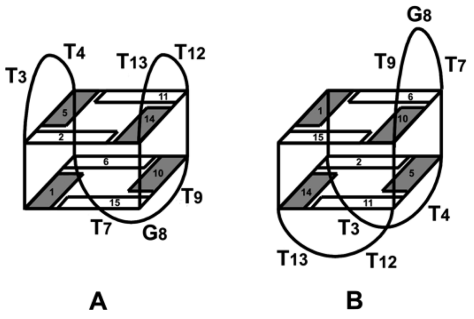


**Figure 1.** Schematic drawings of the X-ray derived G-quadruplex structures of TBA as reported in PDB IDs 1HAO (A) and 1HUT and 1HAP (B). In (A) TT loops span narrow grooves and TGT spans wide grooves, vice versa in (B). White and gray squares indicate G bases in *anti* and *syn* conformation, respectively.

a neighboring thrombin. Thus, according to the adopted folding and the relative orientation with respect to thrombin, TBA bound to ABE I by using the TT loops (PDB ID 1HAO; Figure 1A) or the TGT loop (PDB IDs 1HUT and 1HAP; Figure 1B). A subsequent re-evaluation[8] of the diffraction data of TBA–thrombin complexes[7a,b] evidenced that the NMR-derived folding (Figure 1A) could fit all diffraction data if alternative aptamer orientations with respect to thrombin were considered. Indeed, according to the electron density maps, it was assumed that the oligonucleotide quartet region (including the DNA backbone) was correct as reported in the crystal structures, whereas, due to the D2 symmetry of the aptamer core, there are four distinct possible orientations of the NMR folding that overlap with the core of the X-ray model (Figure 2). The re-evaluation of the X-ray complex gave similar results among orientations I–IV, but orientation III showed the best agreement with the experimental data.[8]

Accordingly, different TBA–thrombin complexes in which the aptamer can bind ABE I through the TGT loop and ABE II through the TT loops (Figure 2, orientations I and II), or the other way around (Figure 2, orientations III and IV), are possible. Supporting this view, the newly released X-ray structures of thrombin–TBA–$Na^+$ and thrombin–TBA–$K^+$ complexes (PDB IDs 4DIH and 4DII, respectively)[7c] showed the aptamer interacting with the enzyme assuming orientation IV (Figure 2). Moreover, the X-ray structure of human thrombin in complex with a modified TBA containing a 5′-5′ inversion of the polarity site (3′GGT5′-5′TGGTGTGGTTGG3′, namely mTBA) has also been reported (PDB ID 3QLP).[9] The X-ray complex revealed that the interaction occurs between the TT loops and ABE I (orientation III in Figure 2), whereas the TGT loop, particularly $T_7$, is not involved in any relevant interaction with the protein. Despite the fact that mTBA binds to thrombin with higher affinity with respect to TBA,[10] it showed poor anticoagulant activity if compared to TBA in PT assay.[11] On the other hand, Toggle-25t, an RNA aptamer that contains 2′-fluoropyrimidine nucleotides, and a 29-mer single-stranded DNA, designated DNA60-18[29] or HD22, bind selectively thrombin at ABE II and they also showed limited effect on clotting times.[12] Because of their thrombin allostery, ABE I and ABE II aptamers were used in combination to test their mixed effect on thrombin activity.[4,13] The obtained results showed that synergistic anticoagulant effects can be achieved by mixing TBA with Toggle-25t or HD22 and by linking TBA to HD22 with an appropriate-sized spacer.

In this scenario, due to the symmetry of TBA and the complexity of the regulatory mechanism of thrombin, which includes a long-range allosteric linkage between ABE I and ABE II,[14,15] the exact binding mode of aptamers to thrombin and its correlation with the observed biological activity is still a matter of debate. Nevertheless, biological results indicated that TBA exerts its anticoagulant activity mainly competing with fibrinogen at ABE I.[16] The phase I clinical trial for TBA demonstrated its positive pharmacokinetic profile in humans; however, clinical trials were halted after phase I due to suboptimal dosing profiles.[17] To optimize its anticoagulant properties, of particular interest is the enlargement of data gathering about TBA structure–activity relationships (SARs) through the development of new derivatives. In the nucleic acids research area the introduction of suitable modifications on natural oligonucleotide sequences represents a method widely employed to explore the relevance of single nucleotides both on secondary structure folding topology and on binding with target proteins. The explored modifications involve the nucleobases,[18] the sugar–phosphate backbone,[19] and the conjugation to flexible non-nucleotide linkers.[20]

In our understanding of the bases of TBA–thrombin recognition, we previously developed new single-stranded TBA analogues, in which the acyclic nucleoside **a** (Figure 3) replaced, one at a time, all thymine residues along the aptamer sequence.[21]

The modification at position 7 in the $T_7G_8T_9$ loop (herein TBA-$T_7$**a**) gives rise to an ON that folds into a quadruplex structure that is more stable and active than the quadruplex structure formed by TBA. On the other hand, within the four ONs containing the acyclic nucleoside **a** at one position of TT loops, the ON modified at $T_{12}$ (herein TBA-$T_{12}$**a**) showed the

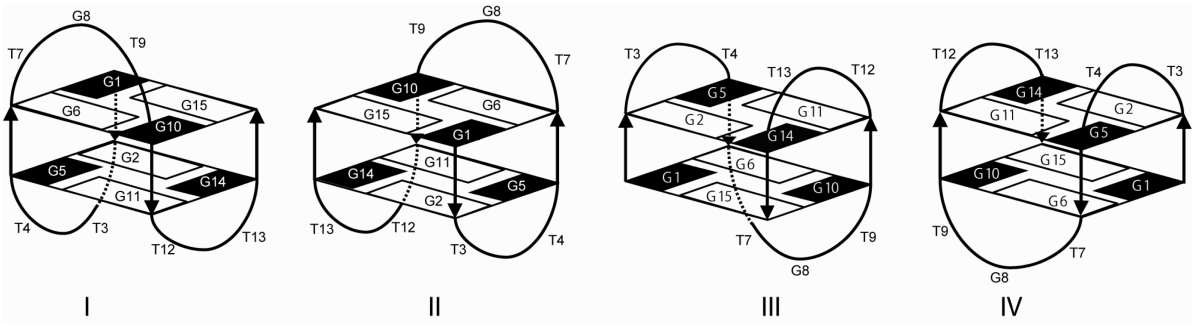


**Figure 2.** Representation of the four orientations of the NMR derived folding with respect to thrombin corresponding to the D2 symmetry of the quadruplex core assuming the same strand polarity of the X-ray complex.


dx.doi.org/10.1021/jm301414f | J. Med. Chem. 2012, 55, 10716–10728

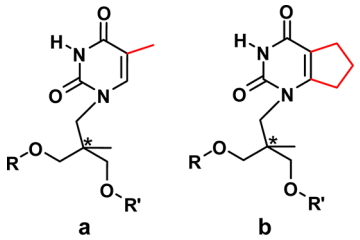

**Figure 3.** Acyclic nucleosides mimicking T. The presence of the carbon atom marked with an asterisk causes the formation of two diastereomeric ONs when the nucleoside is inserted in the TBA sequence.

most significant biological properties.[21] In line with data reported from other authors,[22] our results evidenced that modification at $T_7$ and $T_{12}$ along the TBA sequence can be fruitful to improve the biological activity.

To investigate the role of the modification at $T_7$ and $T_{12}$ in affecting the structural stability and the biological activity, we synthesized two new modified TBAs, named TBA-$T_7$**b** and TBA-$T_{12}$**b**, which differed from the previously reported analogues only in the thymidine base coupled with the acyclic linker, which was bulked by fusing a hydrophobic five member cycle with the pyrimidine ring (**b**, Figure 3). The abilities of TBA-$T_7$**b** and TBA-$T_{12}$**b** to fold into G-quadruplex structures, as well as their biological properties, were evaluated by CD and $^1$H NMR experiments and by PT and purified fibrinogen clotting assays, respectively. Finally, a computational study allowed the analysis of the obtained SARs.

## RESULTS

**Synthesis of Monomer 6.** The synthesis of the modified acyclic nucleoside phosphoramidite building block **6**, used for the automated synthesis of TBA-$T_7$**b** and TBA-$T_{12}$**b**, is summarized in Scheme 1.

The synthesis of N1-alkylated intermediate **3** was performed via Mitsunobu reaction[23] between **2**, obtained as described under Experimental Section, and **1**. The yields of this coupling reaction were strongly dependent on the initial temperature of the system and on the order in which the reagents were added. We found that temperatures lower than 30 °C were always detrimental to the reaction yield, and that higher yields (45−50%) were obtained by mild heating (30 °C) of a dioxane solution containing **2** and triphenylphosphine followed by addition of di-*tert*-butylazodicarboxylate and finally a dioxane solution of protected linker **1** (100 μL of solvent per 1 mmol). The intermediate **4** was obtained by removing both the linker and nucleobase protecting groups from **3** using a one-pot procedure (see Experimental Section). Finally, **4** was functionalized to phosphoramidite buiding block **6** using standard procedure.

The acyclic nucleoside **6** was inserted as a T mimic at position 7 or 12 along the TBA sequence to obtain TBA-$T_7$**b** and TBA-$T_{12}$**b**, respectively.

**Structural Characterization.** TBA-$T_7$**b** and TBA-$T_{12}$**b** were characterized by circular dichroism (CD), CD melting, and $^1$H NMR for their ability to fold into G-quadruplexes. The introduction of the new acyclic nucleoside **b** at position 7 or 12 does not affect the overall G-quadruplex topology formed in solution. CD profiles of TBA-$T_7$**b** and TBA-$T_{12}$**b** are similar to those of TBA in both PBS and $K^+$ buffer (left and right panels, respectively, in Figure 4), showing maxima at about 208, 245, and 295 nm and a minimum at 267 nm. As expected, positive CD bands have higher molar ellipticities in $K^+$ buffer than in PBS, according to the well-known dependence of G-quadruplex stabilities from the type of cations present in the buffer solution.[24]

**Scheme 1. Synthesis of Monomer 6**[a]

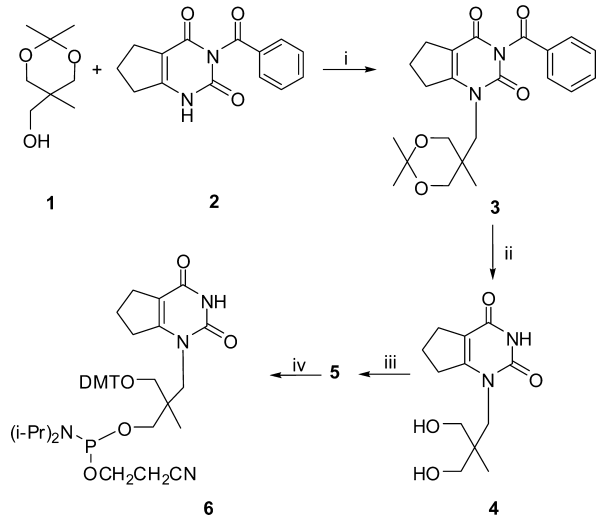

[a](i) **1** 0.94 g (5.9 mmol), **2** 1.50 g (5.9 mmol), triphenylphosphine 2.28 g (8.7 mmol), di-*tert*-butylazodicarboxylate 2.1 g (9.1 mmol), dry dioxane (70 mL), 24 h, 30°C, yields 43%; (ii) (a) **3** 1.0 g (2.5 mmol), Dowex $H^+$ 450 mg, MeOH/$H_2O$ (9:1 v/v) 100 mL; (b) aqueous NaOH (1.0 M, 5 mL) yields 98%; (iii) **4** 640 mg (2.5 mmol), 4,4′-dimethoxytrytylchloride 541 mg (1.6 mmol), 2,4-dimethylaminopyridine 15 mg (0.12 mmol), pyridine (20 mL), acetonitrile (10 mL), 1.5 h, rt, yields 45%; (iv) **5** 600 mg (1.1 mmol), 2-cyanoethyldiisopropylchlorophosphoramidite 300 μL (1.2 mmol), DIPEA 600 μL (3.6 mmol), DCM (8 mL), 40 min, rt, yields 99%.

The $^1$H NMR analysis, performed at temperatures in the range of 25−50 °C, confirmed that TBA-$T_7$**b** and TBA-$T_{12}$**b** form a stable G-quadruplex structure when annealed in $K^+$ buffer. However, $^1$H NMR spectra appear more crowded than expected for a single quadruplex species, even at 25 °C (Figure 5), where only 14 aromatic signals and 8 imino proton signals are expected. This finding was previously explained by considering that the replacement of a T residue with the acyclic nucleoside **a** produces two closely related diastereomeric G-quadruplex forming ONs.[21]

Although both modified ONs show $T_m$ values higher than that of TBA (Figure 6 and Table 1), the replacement of $T_7$ with the acyclic nucleoside **b** stabilizes the resulting G-quadruplexes more efficiently than replacement of $T_{12}$.

**PT Assay.** The anticoagulant activity in the presence of all thrombin substrates and cofactors was evaluated by PT assay. PT analyses were performed at [ON] of 2 and 20 μM after 2 min of incubation with human plasma (Figure 7).

To better understand the effects induced by the presence of nucleoside **b** on the anticoagulant activity, we compared the prolonging of clotting time caused by TBA-$T_7$**b** and TBA-$T_{12}$**b** with that of TBA and those of the previously reported[21] analogues TBA-$T_7$**a** and TBA-$T_{12}$**a** (Table 2).

It is noteworthy that TBA-$T_7$**b** prolonged the basal PT value to a significantly larger extent with respect to TBA and TBA-$T_7$**a** (Figure 7 and Table 2). Replacement of nucleoside **a** for **b** was more effective also at position 12 (Table 2). In particular, TBA-$T_{12}$**b** is less active than TBA at 2 μM, but showed a


dx.doi.org/10.1021/jm301414f | J. Med. Chem. 2012, 55, 10716−10728

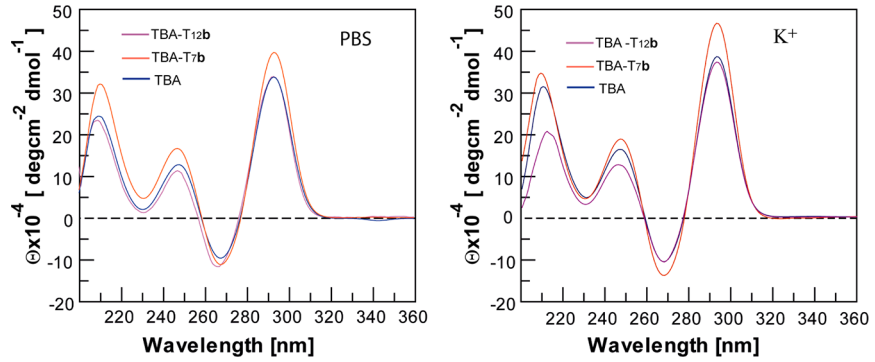


**Figure 4.** CD profiles in PBS (left) and in potassium phosphate buffer (right); [ON] = $2.0 \times 10^{-5}$ M.

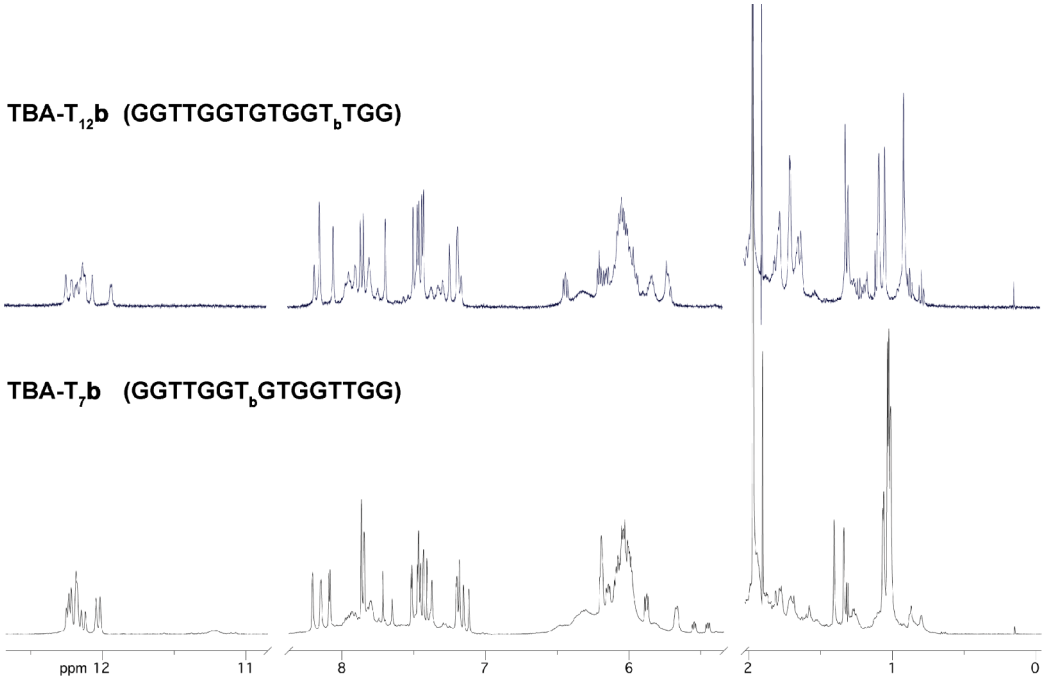


**Figure 5.** $^1$H NMR spectra of TBA-T$_7$**b** and TBA-T$_{12}$**b** recorded at 25 °C in K$^+$ buffer.

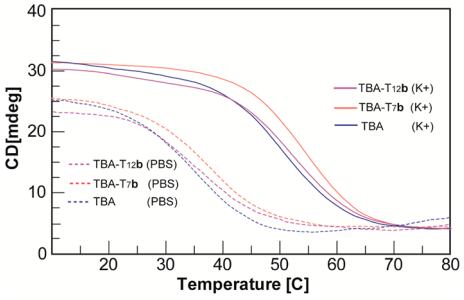


**Figure 6.** CD melting curves of TBA and its analogues in potassium phosphate (continuous lines) or PBS (dotted lines) buffer. Concentration of each ON was $2.0 \times 10^{-5}$ M. The curves were obtained by monitoring the variation of absorbance at 295 nm from 10 to 80 °C at 0.5 °C/min.

greater increase of activity at higher concentration, thus attaining that of TBA at 20 $\mu$M (Figure 7).

To exclude that the observed activity of modified aptamers could be due to higher nuclease stability with respect to TBA, we repeated the experiments, changing the incubation time of TBA and analogues with plasma from 30 s to 15 min. PT results were almost unchanged for all sequences (Supporting Information, Figure 1SI).

**Table 1. $T_m$ Values of TBA and Its Analogues**

| ON | $T_m$ (±0.5 °C) | |
|---|---|---|
| | PBS | K$^+$ buffer |
| TBA | 33.0 | 50.0 |
| TBA-T$_{12}$**a** | 34.0[a] | 51.0[a] |
| TBA-T$_{12}$**b** | 34.5 | 51.5 |
| TBA-T$_7$**a** | 37.5[a] | 54.0[a] |
| TBA-T$_7$**b** | 37.5 | 54.0 |

[a]Data taken from ref 21.

**Fibrinogen Assay Using Human and Bovine Thrombin.** The new ONs were subjected to purified fibrinogen clotting assay to evaluate their ability to inhibit the conversion of soluble fibrinogen into insoluble strands of fibrin in the absence of any other thrombin ligands/effectors (Figure 8 and Tables 1SI and 2SI of the Supporting Information).

The assay was performed using various concentrations of each aptamer. The purified fibrinogen solution was preincubated with the aptamer and the reactions were initiated by the


dx.doi.org/10.1021/jm301414f | J. Med. Chem. 2012, 55, 10716−10728

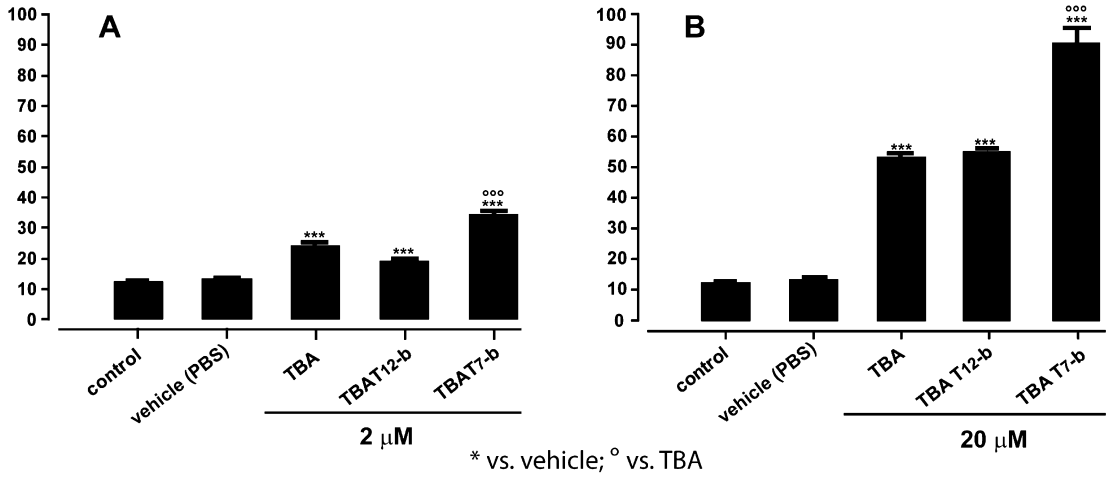


**Figure 7.** Concentration-dependent response, following 2 min ON incubation with human plasma at 2 (A) or 20 $\mu$M (B) [ON]. PT values are expressed in seconds. Each measurement was performed in triplicate and is shown as the mean ± SEM. The basal PT time is 13.4 ± 0.2 s.

**Table 2. PT Values Measured after 2 min of Incubation Using 20 $\mu$M ON Concentration and Fold Increases of Basal PT Time (13.4 ± 0.2 s)**

| ON | PT value[a] (20 $\mu$M) | fold increase |
|---|---|---|
| TBA | 53.68 ± 1.48 | 4.01 ± 0.70 |
| TBA-$T_7$**a** | 60.20 ± 1.38[b] | 4.50 ± 0.60 |
| TBA-$T_7$**b** | 90.60 ± 5.26 | 6.77 ± 0.24 |
| TBA-$T_{12}$**a** | 44.83 ± 1.29[b] | 3.35 ± 0.60 |
| TBA-$T_{12}$**b** | 55.20 ± 0.47 | 4.12 ± 0.20 |

[a]PT values are expressed in seconds. [b]Data taken from ref 21.

addition of human thrombin and clotting times were recorded. The fibrinogen assay results evidenced that at all ON concentrations tested, the most efficient inhibitor is the unmodified TBA sequence (Figure 8A and Table 1SI of the Supporting Information), thus reversing the results gathered from the PT assay. To further investigate this phenomenon, we performed the fibrinogen assay by using bovine thrombin, which differs from human thrombin in some residues of the fibrinogen-binding site (ABE I) that are crucial for TBA–thrombin interaction (see next paragraphs for details). By changing the source of the target enzyme, both modified sequences showed a substantial increase in their ability to inhibit thrombin activity (Figure 8B and Table 2SI of the Supporting Information), whereas the inhibitory activity of TBA was only slightly increased; as a consequence, TBA-$T_7$**b** became again the best inhibitor.

**Conformational Search on TBA and Modified Analogues TBA-$T_7$b and TBA-$T_{12}$b.** An extensive molecular modeling study, including molecular mechanics (MM) and dynamics (MD) calculations, was undertaken to analyze the SARs of new modified TBAs.

In particular, to investigate the conformational properties of TBA and the new modified aptamers, a simulated annealing (SA) procedure followed by MM energy minimization was applied. Following the criteria described under Experimental Section, resulting conformers were analyzed and each nucleotide of loops was classified on the basis of (i) $\chi$ torsional angle values, to identify the conformation of the glycosidic bond (i.e., *syn*, *anti*, or s/a); and (ii) the interatomic distance between its own centroid and that of the two G-tetrads, to investigate the position of loop nucleotides with respect to the

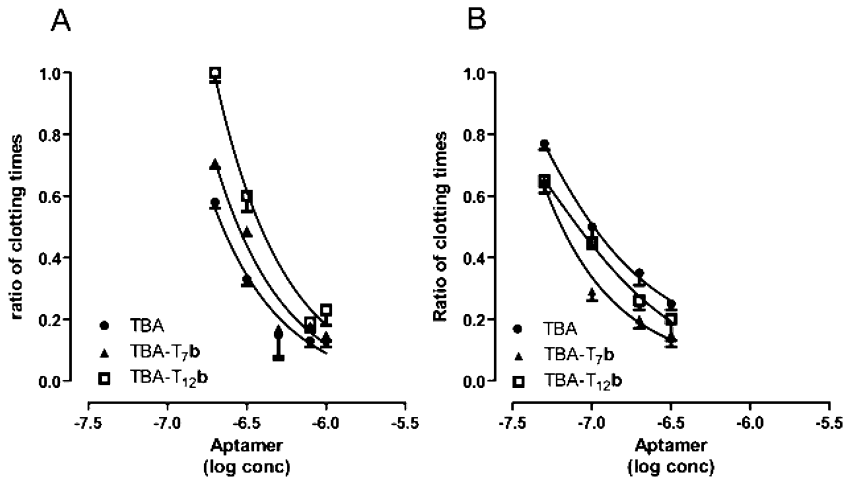


**Figure 8.** Effects of aptamers on human (A) and bovine (B) thrombin clotting time in fibrinogen solution. The results are expressed as the ratio of clotting times measured in the absence and in the presence of the aptamers. The effects are reported as a function of log [ON]. Each measurement was performed in triplicate and is shown as the mean ± SD.


dx.doi.org/10.1021/jm301414f | J. Med. Chem. 2012, 55, 10716–10728

Table 3. Calculated Occurrence Rates (Percent) of *syn*, *anti*, and s/a Conformers of TGT and TT Glycosidic Bonds

| | TBA | | | TBA-$T_7$**b** | | | TBA-$T_{12}$**b** | | |
|---|---|---|---|---|---|---|---|---|---|
| | *syn* | *anti* | s/a | *syn* | *anti* | s/a | *syn* | *anti* | s/a |
| $T_3$ | 28.5 | 69.5 | 2.00 | 37.0 | 61.5 | 1.50 | 47.0 | 50.5 | 2.50 |
| $T_4$ | 38.5 | 56.0 | 5.50 | 29.0 | 65.5 | 5.50 | 43.0 | 52.0 | 5.00 |
| $T_7$[a] | 39.0 | 59.5 | 1.50 | | | | 36.0 | 62.5 | 1.50 |
| $G_8$ | 39.5 | 38.0 | 22.5 | 35.0 | 46.5 | 18.5 | 34.5 | 44.0 | 21.5 |
| $T_9$ | 41.5 | 50.0 | 8.50 | 34.0 | 57.0 | 9.00 | 42.0 | 51.0 | 7.00 |
| $T_{12}$[b] | 32.0 | 66.0 | 2.00 | 42.0 | 56.0 | 2.00 | | | |
| $T_{13}$ | 37.0 | 59.0 | 4.00 | 36.0 | 60.5 | 3.50 | 42.0 | 54.5 | 3.50 |

[a]$T_7$ residue in TBA-$T_7$**b** is replaced by the acyclic nucleoside **b**. [b]$T_{12}$ residue in TBA-$T_{12}$**b** is replaced by the acyclic nucleoside **b**.

guanine planes (i.e., "stacked" or "not-stacked"). Occurrence rates were calculated and compared to those obtained for TBA. Because the replacement of $T_7$ and $T_{12}$ residues with nucleoside **b** produced a mixture of diastereoisomers, characterized by *S* or *R* configuration at the acyclic linker, the occurrence rates reported in Tables 3 and 4 are the mean of the values obtained for the two diastereoisomers; single diastereoisomer values are reported in Tables 3SI and 4SI of the Supporting Information.

Table 4. Calculated Occurrence Rates (Percent) of Conformers Presenting TGT and TT Nucleobases "Stacked" on the Guanine Planes

| | TBA | TBA-$T_7$**b** | TBA-$T_{12}$**b** |
|---|---|---|---|
| $T_3$ | 62.5 | 33.0 | 39.0 |
| $T_4$ | 46.0 | 60.0 | 65.0 |
| $T_7$[a] | 14.0 | 12.0 | 10.0 |
| $G_8$ | 78.5 | 50.0 | 49.0 |
| $T_9$ | 26.0 | 39.5 | 42.5 |
| $T_{12}$[b] | 33.5 | 37.0 | 29.0 |
| $T_{13}$ | 38.0 | 40.5 | 29.0 |

[a]$T_7$ residue in TBA-$T_7$**b** is replaced by the acyclic nucleoside **b**. [b]$T_{12}$ residue in TBA-$T_{12}$**b** is replaced by the acyclic nucleoside **b**.

The structural analysis evidenced that, although inducing some variations, the introduced modifications at $T_7$ and $T_{12}$ did not cause a reversal of the conformational preference of the glycosidic bonds with respect to TBA (Table 3 and Table 3SI of the Supporting Information). Consequently, in agreement with previously reported NMR studies,[6c] TBA and modified aptamers TBA-$T_7$**b** and TBA-$T_{12}$**b** conserved an overall preference for the *anti* conformation of thymines in TGT and TT loops.

With regard to the stacking of the TGT loop nucleobases on the G-tetrads, TBA-$T_7$**b** and TBA-$T_{12}$**b** present an increased stacking of $T_9$ and a decreased stacking of $G_8$ (Table 4 and Table 4SI of the Supporting Information). Nevertheless, the conformational features of the TGT loop still evidenced the same trend of TBA with the following order of residue stacking on the G-tetrads: $G_8 > T_9 > T_7$.

The two modified analogues showed a similar conformational behavior at the $T_3T_4$ loop because, either in TBA-$T_7$**b** or in TBA-$T_{12}$**b**, the rate of stacked conformation of $T_3$ and $T_4$ decreased and increased, respectively, with respect to TBA, evidencing a conformational linkage between TGT and $T_3T_4$ loops. On the contrary, different results were obtained for the $T_{12}T_{13}$ loop. In fact, as expected, the substitution of $T_{12}$ with the acyclic nucleoside **b** (TBA-$T_{12}$**b**) affected the conformational flexibility of the $T_{12}T_{13}$ loop, inducing a decreased stacking rate of both nucleobases, which was not observed in TBA-$T_7$**b** (Table 4 and Table 4SI of the Supporting Information). NMR studies performed on TBA[6a] revealed that the positioning of $T_4$ and $T_{13}$ plays a key role in quadruplex folding and stability; accordingly, due to the increased stacking of $T_4$ and $T_{13}$ on the guanine planes, TBA-$T_7$**b** was structurally more stable than TBA in CD melting experiments (Table 1 and Figure 6).

**Molecular Modeling Studies on Aptamer Interaction with Human and Bovine Thrombin.** With the aim of identifying the effects of the new structural modifications on aptamer–thrombin interactions, first, all possible aptamer–thrombin binding modes and the corresponding binding interactions were analyzed (PDB IDs 1HAO, 1HAP, 1HUT, 4DIH, and 4DII; see Experimental Section). This study revealed that the various binding orientations of TBA with respect to human thrombin (Figures 1 and 2) produced different binding modes in the crystal complexes sharing similar interactions with ABE I but involving different aptamer residues (Figure 9 and Table 5SI of the Supporting Information).

Indeed, a thymine residue of TBA always interacts with ABE I hydrophobic cleft lined by Ile24, His71, Ile79 and Tyr117, but, depending on the binding mode, the interactions involve $T_3$ (Figure 9C,D), or $T_7$ (Figure 9A,B), or $T_{12}$ (Figure 9E,F). $T_7$ interacts penetrating into the hydrophobic cleft more than $T_{12}$ and $T_3$ (Figure 9F vs Figure 9B,D); while the positioning of these latter resulted identical due to the symmetry of the two TT loops (Figure 9B vs Figure 9D). By consequence, a second ABE I subsite, including Gln38, Tyr76 and Ile82, interacts with $T_{12}$ or $T_3$, depending on the binding orientation (Figure 9A–D). When the TGT loop binds to ABE I, the interaction with this second subsite is absent (Figure 9E,F).

Second, to identify the structural differences in TBA-binding site, experimentally determined structures of human and bovine thrombin were compared (PDB IDs are listed in the Experimental Section). Only three TBA-binding site residues, Ile24, Asn78, and Ile79, were mutated in bovine thrombin (Supporting Information, Table 6SI), with no significant variation of the backbone structure (Figure 9). Human thrombin Asn78 residue (replaced by a lysine in bovine thrombin) interacts only with the TGT loop, establishing an H-bond interaction with the phosphate group of $T_9$ (PDB IDs 1HUT and 1HAP; Figure 9E,F and Table 5SI of the Supporting Information). On the contrary, the interactions with human ABE I hydrophobic cleft containing Ile24 and Ile79 are conserved in all crystal complexes and involve $T_3$ or $T_7$ or $T_{12}$ depending on TBA-binding orientation (Figure 9 and Table 5SI of the Supporting Information). The replacement of these two isoleucine residues in human thrombin by two valine residues in the bovine homologue determines an enlargement of the employable volume within the ABE I cleft.


dx.doi.org/10.1021/jm301414f | J. Med. Chem. 2012, 55, 10716–10728

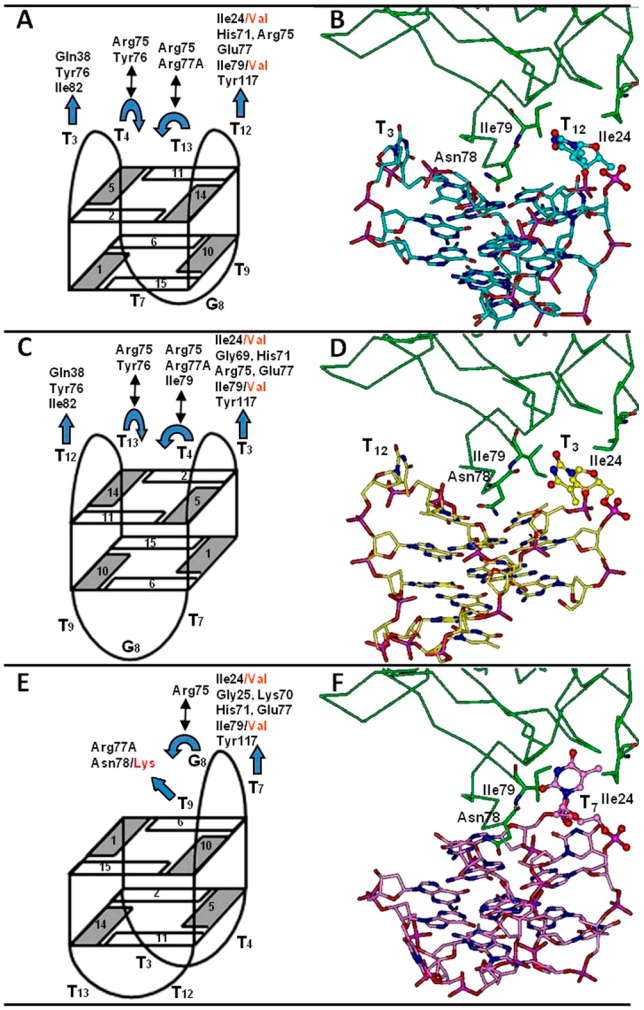


**Figure 9.** Cartoon (left) and 3D (right) structure of the different binding orientations of TBA with respect to human thrombin ABE I (green). (A, C, and E) Amino acid residues involved in TBA–thrombin interactions are evidenced in black; where mutated, the corresponding bovine residues are reported in red. The blue curve and straight arrows indicate loop nucleotides "stacked" or "not-stacked" on G-tetrad, respectively. (B) PDB ID 1HAO (TBA carbons = cyan); (D) PDB ID 4DIH (TBA carbons = yellow); (F) PDB ID 1HAP (TBA carbons = magenta). Protein carbons are colored in green, residues within TBA binding site that are mutated in bovine thrombin are shown and labeled. The nucleotides $T_3$, $T_7$, and $T_{12}$ are evidenced as ball and stick. Heteroatoms are colored as follows: O = red; N = blue; P = magenta. Hydrogens are omitted for the sake of clarity.

We then calculated the occurrence rates of TBA, TBA-$T_7$**b**, and TBA-$T_{12}$**b** SA/MM conformers presenting solvent-accessible surface areas of residues 3, 7, and 12 equal to or greater than that of the corresponding residue of TBA binding the ABE I hydrophobic cleft in experimentally determined complexes (Table 5; single diastereoisomer values are reported in Table 7SI of the Supporting Information).

Interestingly, the replacement of $T_7$ and $T_{12}$ with the acyclic nucleoside **b** determined in both cases a greater rate of conformations presenting a solvent-exposed conformation. Moreover, in agreement with the results reported in Tables 3 and 4, $T_3$ is more exposed to the solvent in the new modified aptamers than in TBA.

Finally, we calculated the occurrence rates of bioactive conformations of residues at positions 3, 7, and 12 resulting from SA/MM calculations on TBA, TBA-$T_7$**b**, and TBA-$T_{12}$**b** (Figure 10 and Table 6; single diastereoisomer values are reported in Table 8SI of the Supporting Information).

**Table 5. Occurrence Rates (Percent) of TBA, TBA-$T_7$b, and TBA-$T_{12}$b SA/MM Conformers Presenting a Solvent-Accessible Surface Area (Å$^2$) of Residues 3, 7, and 12 Equal to or Greater than That of the Corresponding Residue of TBA Assuming the Bioactive Conformation at the ABE I Hydrophobic Cleft**

| ON | $T_3$ | $T_7$[a] | $T_{12}$[b] |
|---|---|---|---|
| TBA | 16.5 | 85.0 | 36.5 |
| TBA-$T_7$**b** | 21.0 | 88.0 | 34.5 |
| TBA-$T_{12}$**b** | 22.0 | 76.0 | 50.0 |

[a]$T_7$ residue in TBA-$T_7$**b** is replaced by the acyclic nucleoside **b**. [b]$T_{12}$ residue in TBA-$T_{12}$**b** is replaced by the acyclic nucleoside **b**.

With this aim, all obtained conformers were superimposed on the experimentally determined TBA–thrombin complexes by fitting the guanine tetrads to evaluate the overlap with the residue interacting with the ABE I hydrophobic cleft (see Experimental Section for details). Obtained results show that TBA-$T_7$**b** presents an increased rate of bioactive conformations if compared to TBA; on the contrary, the substitution of $T_{12}$ with **b** decreases the rate of bioactive conformations of $T_3$ and $T_7$.

Interestingly, the replacement of $T_7$ and $T_{12}$ with the acyclic nucleoside **b** determined in both cases a greater rate of conformations presenting a solvent-exposed position able to drive the interaction with the ABE I hydrophobic cleft. Nevertheless, likely due to the higher flexibility of the TGT loop with respect to the TT loops, there is a higher occurrence rate of $T_7$**b** assuming the ABE I bioactive conformation compared to $T_3$ and $T_{12}$**b** (Table 6 and Figure 10).

## DISCUSSION

The introduction of a bulky five member cycle on the pyrimidine ring of the modified thymine residues of TBA-$T_7$**a** and TBA-$T_{12}$**a** led to compounds (TBA-$T_7$**b** and TBA-$T_{12}$**b**) able to fold into G-quadruplexes characterized by unaffected structural stability but showing different anticoagulant activity with respect to their parent compounds.[21] Because TBA-$T_7$**b** and TBA-$T_7$**a** show the same melting profile, with a $T_m$ higher than that of TBA (Table 1), it can be concluded that the sole presence of the acyclic linker unit at position 7 is responsible for the structural stabilizing effect. Conformational analysis results indicate that the introduction of the acyclic linker at position 7 increased the solvent-exposed surface area (Table 6) of the modified residue and the rate of $T_4$ and $T_{13}$ conformations stacked on the guanine planes (Table 4). These data account for the nucleobase 7 always positioned outside the G-quadruplex core and not involved in intramolecular interactions, as well as for the reported stabilizing role played by $T_4$ and $T_{13}$ on TBA structural stability.[6] In line with our results, a similar increase in $T_m$ value has also been observed by replacing the sugar moiety of $T_7$ with a different acyclic linker.[22] Interestingly, the fact that TBA-$T_7$**a** and TBA-$T_7$**b** showed the same enhancement of the $T_m$ value with respect to TBA is not correlated with their diverse anticoagulant activities. Indeed, although the anticoagulant activities of TBA-$T_7$**a** and TBA-$T_7$**b** are higher than that of TBA, TBA-$T_7$**b** is more active than TBA-$T_7$**a** (Figure 7). Furthermore, PT assay data show that the incorporation of


dx.doi.org/10.1021/jm301414f | J. Med. Chem. 2012, 55, 10716–10728

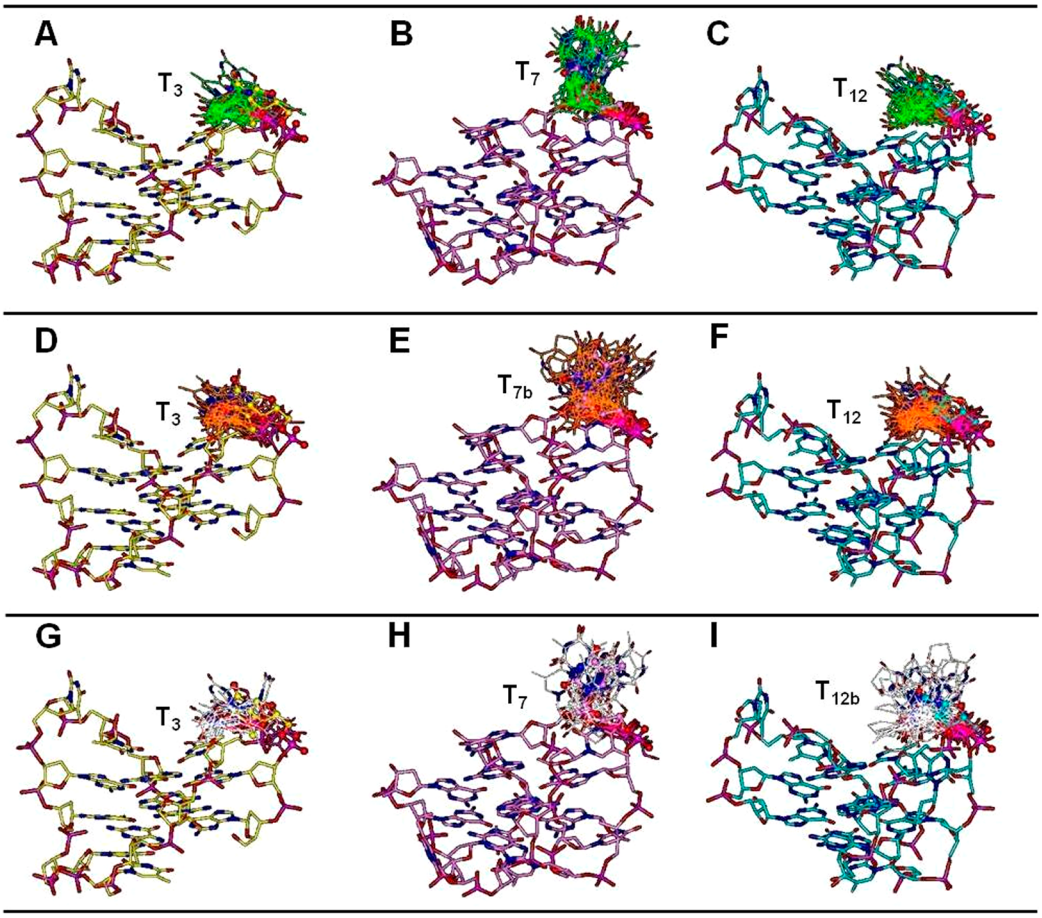


**Figure 10.** TBA (green; A–C), TBA-$T_7$**b** (orange; D–F), and TBA-$T_{12}$**b** (white; G–I) SA/MM conformers presenting residue 3, 7, or 12 assuming ABE I hydrophobic cleft binding conformation. Molecular models are superimposed on 4DIH (A, D, G; yellow), 1HAP (B, E, H; pink), or 1HAO (C, F, I; cyan) by fitting the guanine tetrads. All conformers of TBA and the mean of those obtained for the two diastereoisomers of TBA-$T_7$**b** and TBA-$T_{12}$**b** are shown. For the sake of clarity only the residue interacting with the ABE I hydrophobic cleft is displayed and hydrogens are omitted. Heteroatoms are colored as follows: O = red; N = blue; P = magenta.

**Table 6. Occurrence Rates (Percent) of Bioactive Conformations at the ABE I Hydrophobic Cleft of Residues at Positions 3, 7, and 12 Resulting from SA/MM Calculations**

| ON | $T_3$ | $T_7$[a] | $T_{12}$[b] |
|---|---|---|---|
| TBA | 9.50 | 12.0 | 10.0 |
| TBA-$T_7$**b** | 8.00 | 14.0 | 13.5 |
| TBA-$T_{12}$**b** | 6.50 | 6.50 | 10.0 |

[a]$T_7$ residue in TBA-$T_7$**b** is replaced by the acyclic nucleoside **b**. [b]$T_{12}$ residue in TBA-$T_{12}$**b** is replaced by the acyclic nucleoside **b**.

nucleoside **b** was more effective than that of nucleoside **a** also at position 12 of TBA (Table 2). It was somehow surprising that the activity of TBA with respect to the new modified analogues is reversed in fibrinogen assay (Figure 8A). It could be supposed that the introduction of an acyclic linker in the TBA phosphate backbone enhances the aptamers' stability to nucleases, thus producing an increment of inhibitory effect in plasma tests. However, PT results were almost unaffected upon increasing of the incubation time of all sequences with plasma (Supporting Information, Figure 1SI), thus suggesting that, in the explored conditions, nuclease stabilities and inhibitory activities are uncorrelated and that modifications at $T_7$ directly affect the interaction of aptamers with thrombin. Supporting this view, the use of bovine thrombin in fibrinogen assay changed again the activity trend. In particular, when tested toward bovine thrombin, the inhibitory activity of TBA-$T_7$**b** and TBA-$T_{12}$**b** significantly increases, becoming much higher than that of TBA, which, on the contrary, is almost unchanged in both fibrinogen tests (Figure 8, panel A vs panel B). On this ground, subtle structural differences between human and bovine thrombin that specifically affect the binding with TBA-$T_7$**b** and TBA-$T_{12}$**b** must exist. The results from our molecular modeling study using both human and bovine thrombin revealed that the obtained SARs fit with the binding of modified nucleobases, $T_7$**b** and $T_{12}$**b** to thrombin ABE I. Indeed, within the TBA binding site, human thrombin differs from the bovine counterpart by only three amino acids located at ABE I (Supporting Information, Table 6SI). Specifically, in the bovine enzyme two isoleucine residues are replaced by valine residues and an asparagine is mutated into a lysine. In the reported human thrombin–TBA complexes, the isoleucine residues are involved in hydrophobic contacts with $T_3$ or $T_7$ or $T_{12}$, depending on the binding orientation of the aptamer (Figure 9). On the other hand, the asparagine residue is involved in H-bond interactions with the phosphate group linking $G_8$ to $T_9$ only when the TGT loop binds to ABE I (Supporting Information, Tables 5SI and 6SI). In the new TBA derivatives TBA-$T_7$**b** and TBA-$T_{12}$**b**, the introduction of the acyclic linker facilitates the extension of the phosphate


dx.doi.org/10.1021/jm301414f | J. Med. Chem. 2012, 55, 10716–10728

backbone toward the solvent and the penetration of the modified nucleobase within the ABE I hydrophobic cleft, thus amplifying the steric hindrance caused by the presence of the five member cycle on modified nucleobase **b** (Table 5 and Figure 10). Accordingly, the presence of the smaller Val24 and Val79 residues in bovine thrombin could explain the increased activity of the new modified TBA analogues for this enzyme. The observed higher activity of TBA-$T_7$**b** is indeed correlated to the calculated higher rate of bioactive conformations at the ABE I hydrophobic cleft with respect to TBA and TBA-$T_{12}$**b** (Table 6 and Figure 10). This hypothesis is supported by the previously reported activity of TBA-$T_7$**a** and TBA-$T_{12}$**a**,[21] which, lacking the steric bulk at the modified nucleoside, was more active in the fibrinogen assay using human thrombin. On the other hand, the charged group at the lysine side chain allows the establishment of an ionic interaction with the modified TGT phosphate backbone of TBA-$T_7$**b**, likely contributing to the enhancement of inhibitory ability.

On these bases, the apparent incongruence of PT and fibrinogen assay results, using human thrombin, can be interpreted by taking into account the effects of different aptamer binding modes on thrombin allostery.[2] In the PT assay a number of thrombin ligands/effectors other than fibrinogen that are able to modulate thrombin activity are present,[1,2,14,25,26] thus driving different binding modes; the new modified aptamers could differently affect this ligand/effector binding network. In this scenario, it is noteworthy that the 65−84 thrombin loop, involved in specific interactions with the modified nucleobase of the new TBA derivatives according to our binding mode hypothesis, has been proved to be responsible for the allosteric long-range communication among ABE I, the catalytic site, and ABE II.[2e,15]

Altogether, our results reveal the absence of a direct correlation between the structural stability and the anticoagulant property in our series of modified TBAs, suggesting that the role played by $T_7$ (placed in the TGT loop) and $T_{12}$ (placed in the TT loop close to the 3′ terminus) in the biological activity of TBA and its analogues could involve alternative aptamer binding modes and the complex and not yet fully understood allosteric mechanism of action of thrombin.

## CONCLUSIONS

Bringing together the so far acquired knowledge of the thrombin−TBA interaction and thrombin allosteric regulatory mechanism with our SAR data, we determined that the G-quadruplexes formed by the modified TBAs can bind the thrombin ABE I hydrophobic cleft by using either TGT or one of the two TT loops. Our results indicate that the incoherency of their behaviors in the two explored biological tests is due to the molecular process through which they exert the anticoagulant activity, which is surely more intricate than a competitive inhibition with the fibrinogen-binding site. Besides their high anticoagulant activity, these molecules represent valuable tools to further explore the complex regulatory mechanism of thrombin during plasma coagulation that is, as yet, not completely clarified.

## EXPERIMENTAL SECTION

**General Procedure.** Chemicals and anhydrous solvents were purchased from Fluka-Sigma-Aldrich. TLCs were run on Merck silica gel 60 F254 plates. Silica gel chromatography was performed by using Merck silica gel 60 (0.063−0.200 mm). An API 2000 (Applied Biosystem) mass spectrometer was used to perform the analyses of the intermediates and monomer **6**. NMR experiments were recorded using Varian Mercury Plus 400 MHz and Varian $^{UNITY}$INOVA 500 and 700 MHz spectrometers and processed using the Varian VNMR software package. Reagents and phosphoramidites for DNA synthesis were purchased from Glenn Research. ON syntheses were performed on a PerSeptive Biosystem Expedite DNA synthesizer. HPLC purifications and analyses were carried out using a JASCO PU-2089 Plus HPLC pump equipped with a JASCO BS-997-01 UV detector. The purity of the final products was determined as >95% by using a C-18 RP analytical column (C-18 Purospher STAR, Merck) eluted by a gradient of $CH_3OH$ in $H_2O$ (from 0 to 100% in 30 min). CD experiments were performed on a JASCO 715 spectropolarimeter equipped with a PTC-348 temperature controller.

**Synthesis of Monomer 6.** *(a) 3-Benzoyl-6,7-dihydro-1H-cyclopenta[d]pyrimidine-2,4(3H,5H)-dione (**2**).* Nucleobase 6,7-dihydro-1*H*-cyclopenta[*d*]pyrimidine-2,4(3*H*,5*H*)-dione was obtained as previously reported by Renault et al.[27] and converted in its N3 benzoyl derivative **2**.[21] $^1$H NMR (400 MHz; mixture of $CD_3OD$ and $CDCl_3$), $\delta$ 7.75 (d, $J$ = 8.0 Hz, 2H), 7.60 (t, $J$ = 8.0 Hz, 1H), 7.43 (t, $J$ = 8.0 Hz, 2H), 3.03 (t, $J$ = 7.3 Hz, 2H), 2.67 (t, $J$ = 7.3 Hz, 2H), 2.10 (q, $J$ = 7.3 Hz, 2H); $^{13}$C NMR (100 MHz; mixture of $CD_3OD$ and $CDCl_3$), $\delta$ 169.3, 166.3, 155.2, 147.3, 134.2, 132.2, 128.9, 128.3, 127.5, 127.0, 113.4, 34.8, 30.5, 18.0. ESI mass (positive mode), calculated 256.1; found 257.1 $[M + H]^+$, 279.1 $[M + Na]^+$.

*(b) 3-Benzoyl-1-[(2,2,5-trimethyl-1,3-dioxan-5-yl)methyl]-6,7-dihydro-1H-cyclopenta[d]pyrimidine-2,4(3H,5H)-dione (**3**).* Compound **2** (1.5 g, 5.9 mmol) was suspended in 70 mL of dry dioxane at 30 °C in the presence of triphenylphosphine (2.28 g, 8.7 mmol) before the addition of di-*tert*-butyl azodicarboxylate (2.1 g, 9.1 mmol). To the resultant mixture, after 10 min of stirring at room temperature, was added 5.9 mmol of **1** dissolved in dry dioxane (300 $\mu$L). The reaction mixture was stirred at room temperature for 18 h under argon. The solution was concentrated under reduced pressure and the residue purified by column chromatography on silica gel eluted with 95:5 $Et_2O/CH_2Cl_2$ to give **3** as a white solid (yield 43%, $R_f$ 0.70). $^1$H NMR (400 MHz; $CDCl_3$), $\delta$ 7.98 (d, $J$ = 8.0 Hz, 2H), 7.60 (t, $J$ = 8.0 Hz, 1H), 7.43 (t, $J$ = 8.0 Hz, 2H), 4.0 (bs, 2H), 3.62 (m, 4H), 3.03 (t, $J$ = 7.3 Hz, 2H), 2.66 (t, $J$ = 7.3 Hz, 2H), 2.09 (q, $J$ = 7.3 Hz, 2H), 1.38 (s, 3H), 1.42 (s, 3H), 0.87 (s, 3H). ESI mass (positive mode), calculated 398.2; found 399.2 $[M + H]^+$, 421.2 $[M + Na]^+$.

*(c) 1-(3-Hydroxy-2-(hydroxymethyl)-2-methylpropyl)-6,7-dihydro-1H-cyclopenta[d]pyrimidine-2,4(3H,5H)-dione (**4**).* Compound **3** (1.0 g, 2.5 mmol) was suspended in 9:1 MeOH/$H_2O$ (100 mL) containing 450 mg of Dowex 50WX8 ($H^+$). After 8 h at room temperature, a NaOH 0.5 M aqueous solution was slowly added to neutralization. The solution was filtered and, in turn, basified with NaOH 1.0 M (5 mL) to remove the N-3 benzoyl group from the nucleobase. After 12 h at room temperature, the pH of the reaction was neutralized, the solvent was evaporated under vacuum, and the residue was dissolved in MeOH and purified by HPLC (C-18 reverse-phase column, Grace Davison Discovery Sciences, eluted with ACN in $H_2O$ from 0 to 50% in 30 min) to give **4** as a white solid (yield 98%, elution time 15 min). $^1$H NMR (700 MHz; $CD_3OD$), $\delta$ 3.80 (bs, 2H), 3.41 (d, $J$ = 11.4 Hz, 2H), 3.38 (d, $J$ = 11.4 Hz, 2H), 3.03 (t, $J$ = 7.3 Hz, 2H), 2.66 (t, $J$ = 7.3 Hz, 2H), 2.09 (q, $J$ = 7.3 Hz, 2H), 0.87 (s, 3H); $^{13}$C NMR (175 MHz; $CD_3OD$), $\delta$ 163.8, 161.4, 155.7, 113.6, 66.6, 49.5, 44.0, 34.2, 28.2, 22.6, 17.8; NOESY (700 MHz; $CD_3OD$), fundamental NOE signal between 3.80 and 3.03 ppm that confirms the linker at the 1N position. ESI mass (positive mode), calculated 254.1; found, 255.3 $[M + H]^+$, 277.3 $[M + Na]^+$, 293.2 $[M + K]^+$.

*(d) 3-(Bis(4-methoxyphenyl)(phenyl)methoxy)-2-((2,4-dioxo-3,4,6,7-tetrahydrohydro-1H-cyclopenta[d]pyrimidin-1-yl)methyl)-2-methylpropyl-2-cyanoethyl Diisopropylphosphoramidite (**6**).* Compound **4** (640 mg, 2.5 mmol), 4,4′-dimethoxytrytyl chloride (541 mg, 1.6 mmol), and 4-dimethylaminopyridine (15.0 mg, 0.12 mmol) were dissolved in dry pyridine (20 mL) and dry ACN (10 mL). The resulting solution was stirred at room temperature under argon for 1.5 h. Dry methanol (200 $\mu$L) was then added to quench the reaction. After 30 min under stirring, the solution was concentrated under reduced pressure and the residue purified by column chromatography

on silica gel (eluted with 50:50:1 EtOAc/hexane/$Et_3N$) to give monodimethoxytritylated **5** as a clear yellow solid (44% yield from **4**; $R_f$ 0.51 in EtOAc/hexane 1:1 v/v). The solid (600 mg, 1.1 mmol) was dried in vacuo overnight before being dissolved in anhydrous DCM (8 mL) and diisopropylethylamine (600 μL, 3.6 mmol) under argon. Three hundred microliters of β-cyanoethyl diisopropylchlorophosphoramidite was then added (1.2 mmol). After 40 min, the reaction was quenched by the addition of dry methanol (100 μL), diluted with ethyl acetate (15 mL), and finally washed with 10% sodium carbonate solution (15 mL) and brine (15 mL). The organic layer was dried on magnesium sulfate and concentrated in vacuo. The residue was purified by silica gel chromatography eluted with DCM, ethyl acetate, and triethylamine (80:10:10). The fractions containing the product were collected and concentrated under vacuum, yielding **6** as a white foam (99% yield; $R_f$ 0.65 in $CHCl_3$/MeOH/TEA 97:3:0.05 v/v/v). $^1$H NMR (700 MHz; $CDCl_3$), δ 7.90 (2H), 7.38 (2H), 7.35 (4H), 7.12 (1H), 6.85 (4H), 3.90 (2H), 3.70 (6H), 3.65 (2H), 3.60 (2H), 3.45 (2H), 3.39−3.02 (4H), 2.60−2.45 (4H), 2.16 (2H), 1.45 (3H), 1.09 (6H), 1.04 (6H); $^{13}$C NMR (175 MHz; $CDCl_3$), δ 158.6, 151.6, 147.3, 139.4, 135.1, 130.3, 129.1, 127.8, 127.7, 127.1, 113.1, 64.4, 60.4, 55.2, 47.3, 33.6, 29.7, 27.6, 20.9, 19.3, 17.3; $^{31}$P NMR (202 MHz, $CDCl_3$), δ 146.1 and 145.9. ESI mass (positive mode), calculated 756.3; found 757.9 $[M + H]^+$, 779.9 $[M + Na]^+$.

**Synthesis of Oligomers.** TBA and analogues were synthesized by using standard solid phase DNA chemistry on controlled pore glass (CPG) support following the β-cyanoethyl phosphoramidite method. The oligomers were detached from the support and deprotected by treatment with an aqueous ammonia solution (33%) at 55 °C overnight. The combined filtrates and washings were concentrated under reduced pressure, dissolved in $H_2O$, and purified by HPLC using an anionic exchange column eluted with a linear gradient (from 0 to 100% B in 30 min) of phosphate buffer at pH 7.0 (A, 20 mM $NaH_2PO_4$ aqueous solution containing 20% $CH_3CN$; B, 1.0 M NaCl, 20 mM $NaH_2PO_4$ aqueous solution containing 20% $CH_3CN$). The oligomers were successively desalted by molecular exclusion chromatography on Biogel P-2 fine. The purity was checked on HPLC by using reverse phase column (Supporting Information, Figure 2SI). The concentrations of the samples used in CD and UV experiments were determined by measuring the absorbance at 260 nm at 80 °C and using the open access program available on http://basic.northwestern.edu/biotools/OligoCalc.html.[28]

**NMR Experiments.** 1D NMR spectra were acquired as 16384 data points with a recycle delay of 1.0 s at temperatures in the range of 2−50 °C. Data sets were zero filled to 32768 points prior to Fourier transformation and apodized with a shifted sine bell squared window function. The pulsed-field gradient DPFGSE[29] sequence was used for $H_2O$ suppression. NMR samples of TBA-$T_7$**b** and TBA-$T_{12}$**b** (0.5 mM single-strand concentration) were prepared in 100 mM $K^+$ buffer ($H_2O/D_2O$ 9:1 v/v containing 90 mM KCl, 10 mM $KH_2PO_4$, and 0.2 mM EDTA).

**CD Experiments.** To perform CD experiments, each ON was dissolved in the potassium (90 mM KCl, 10 mM $KH_2PO_4$, pH 7.0) or PBS (Sigma-Aldrich; 10 mM phosphate buffer, 2.7 mM KCl, 137 mM NaCl, pH 7.4) phosphate buffer at the final ON concentration of $2.0 \times 10^{-5}$ M and submitted to the annealing procedure (heating at 90 °C and slowly cooling at room temperature). Before each experiment, the samples were equilibrated at 10 °C for 30 min. CD spectra were recorded from 200 to 360 at 100 nm/min scanning rate, 16 s response, and 1.0 nm bandwidth. Each CD profile was obtained by taking the average of three scans from which the spectrum of background buffer was subtracted. CD melting curves were obtained by monitoring the variation of absorbance at 295 nm from 10 to 80 °C. Two melting experiments for each ON were recorded at 0.5 °C/min heating rate.

**Prothrombin (PT) Time.** PT time was measured by using a Koagulab MJ Coagulation System with a specific kit RecombiPlas Tin HemosIL (Instrumentation Laboratories, Lexington, MA, USA). The procedure was performed according to the manufacturer's instructions. In our experimental protocol a time course of each ON or vehicle incubated with 100 μL of plasma at 37 °C has been performed. For the evaluation of PT at 20.0 μM, in the apposite microtube, 2.0 μL of the corresponding ON solution ($1.0 \times 10^{-3}$ M in PBS) or vehicle was added. The PT at final ON concentration of 2.0 μM was determined by using 2.0 μL of a diluted ON solution (the initial ON solution $1.0 \times 10^{-3}$ M in PBS was diluted at a final concentration of $1.0 \times 10^{-4}$ M). Using six different incubation times from 30 s to 15 min (i.e., 30 s and 1, 2, 5, 10, and 15 min) 200 μL of the kit solution containing Recombiplastin was added with consequent activation of extrinsic pathway. The PT measurement, for each incubation time, was produced in triplicate, and the average and its standard error values were calculated. The basal clotting time was determined by measuring the clotting time in the absence of any ON. The fold increase of basal PT time was calculated as the ratio between the measured PT time in the presence of each ON and the basal PT value (13.4 ± 0.2 s).

**Purified Fibrinogen Clotting Assay.** ONs were incubated for 1 min at 37 °C in 200 μL of buffer (20 mM tris acetate, 140 mM NaCl, 2.7 mM KCl, 1.0 mM $MgCl_2$, 1.0 mM $CaCl_2$, pH 7.4) containing 2.0 mg/mL of fibrinogen (fibrinogen from human plasma, F 3879, Sigma-Aldrich). One hundred microliters of human (Sigma-Aldrich, T8885, human thrombin suitable for thrombin time test) or bovine (HemosIL, Thrombin Time Kit, Instrumentation Laboratories) thrombin (10 NIH per mL) was then added to the solution containing the fibrinogen and the ON. The time required to clot was measured using a Koagulab MJ Coagulation System. The clotting time of each ON was determined in triplicate at different concentrations. The basal clotting time was determined by measuring the clotting time in the absence of any ONs. Prolonged clotting time was obtained by subtracting the basal clotting value from each ON clotting time. The ratio of basal and prolonged clotting time versus log [ON] was reported.

**Molecular Modeling.** Molecular modeling calculations were performed on SGI Origin 200 8XR12000 and E4 Server Twin 2 x Dual Xeon 5520, equipped with two nodes. Each node was 2 x Intel Xeon QuadCore E5520, 2.26 GHz, 36 GB RAM. The molecular modeling graphics were carried out on SGI Octane 2 workstations.

*(a) Conformational Analysis.* Experimentally determined structures of TBA alone (PDB ID 148D) and in complex with thrombin (PDB IDs 1HAO, 1HAP, and 1HUT) were downloaded from Protein Data Bank (PDB, http://www.rcsb.org/pdb/) and analyzed using the Homology module of Insight 2005 (Accelrys Software Inc., San Diego, CA, USA). Hydrogens were added to all of these structures considering a pH value of 7.4 (Biopolymer Module, Insight 2005).

Because the replacement of $T_7$ and $T_{12}$ residues with nucleoside **b** produced a mixture of diastereoisomers characterized by *S* or *R* configuration at the acyclic linker, for each new TBA analogue TBA-$T_7$**b** and TBA-$T_{12}$**b**, the two diastereoisomers were built by modifying the experimentally determined structure of TBA in complex with thrombin (PDB ID 1HAO; Insight2005 Builder module). Atomic potentials and charges were assigned using the CVFF force field.[30]

The conformational space of TBA (PDB ID 1HAO) and the new modified analogues was sampled through 200 cycles of simulated annealing (SA) followed by molecular mechanics (MM) energy minimization. During the SA procedure, the temperature is altered in time increments from an initial temperature to a final temperature by adjusting the kinetic energy of the structure (by rescaling the velocities of the atoms). The following protocol was applied: the system was heated to 1000 K over 2000 fs (time step of 1.0 fs); a temperature of 1000 K was applied to the system for 2000 fs (time step of 1.0 fs) to surmount torsional barriers; successively, the temperature was linearly reduced to 300 K in 1000 fs (time step of 1.0 fs). Resulting conformations were then subjected to MM energy minimization within Insight 2005 Discover_3 module (CVFF force field) until the maximum rms derivative was <0.001 kcal/Å, using a conjugate gradient[31] as the minimization algorithm.

To reproduce the physiological environment where these molecules act and, to evaluate the effects of the implicit solvent, we sampled the conformational space through the combined procedure of SA/MM calculations, using the dielectric constant of the water ($\varepsilon = 80r$). Moreover, to allow a complete relaxation of the structures preserving the monomolecular chairlike G-quadruplex folding topology, during

the entire course of SA/MM calculations, we applied a tether force of 100 kcal/Å$^2$ to the guanine bases of two quartets.

All resulting conformers were subsequently analyzed and loop nucleotides were classified on the bases of (i) glycosidic bond $\chi$ values, that is, $0° < \chi < 90°$ = *syn*; $-60° < \chi < -180°$= *anti*;[32] $90° < \chi < 180°$ and $-60° < \chi < 0°$ = s/a); (ii) the interatomic distance between the centroid of the ring atoms of the nucleobase of each loop nucleotide and the centroid of the ring atoms of the nucleobases of the two G-tetrads (Pseudo_Atom Define command, Biopolymer Module, Insight 2005). According to the latter parameter, the loop nucleotide was classified as "stacked" when the distance was <8 Å or as "not-stacked" when the distance was >12 Å, whereas a 3D visual inspection was needed to classify the nucleotide as "stacked" or "not-stacked" when the distance was between 8 and 12 Å. A nucleotide termed "stacked" presented at least one nucleobase atom shielded by the G-tetrads; a nucleotide termed "not-stacked" presented no atoms shielded by the G-tetrads. Occurrence rates were calculated for TBA and for each diastereoisomer of the new analogues TBA-$T_7$**b** and TBA-$T_{12}$**b**. Because all experimental data refer to the mixture of the two diastereoisomers, the mean of the values obtained for the two diastereoisomers was also calculated.

*(b) Structural and Bioinformatics Analysis.* To analyze the binding modes of TBAs and the corresponding aptamer−thrombin interactions, all of the experimentally determined structures of aptamers in complex with human thrombin were downloaded from Protein Data Bank: 1HAO, 1HAP, 1HUT, 3DD2, 3QLP, 4DIH, and 4DII. On the other hand, to identify the structural differences in TBA binding site between human and bovine thrombin, additional structures of human (PDB IDs 1HXF, 1TB6, 1TMT, 1TMU, 1XMN, 3HTC, and 4HTC) and bovine (PDB IDs 1HRT, 1VIT, and 3PMA) thrombin, sharing similar ABE I and ABE II ligands, were selected and analyzed. Hydrogens were added to all of the PDB structures considering a pH value of 7.4 (Biopolymer Module, Insight 2005). All structures were superimposed by C$\alpha$ atoms, and their sequences were extracted using the Homology module of Insight 2005 (Accelrys). On the other hand, the human (entry P00734) and bovine (entry P00735) prothrombin sequences were downloaded from the UniProt Knowledgebase (http://www.uniprot.org), and the sequence alignments were performed using Multiple_Sequence Alignment pulldown in the Insight 2005 Homology module. Moreover, for each ligand/enzyme complex, a subset around the ligands that consisted of all residues and water molecules having at least one atom within a 6 Å radius from any given ligand atom was defined. The created subsets were displayed and analyzed through a 3D visual inspection. The results of this analysis were compared with those obtained through the sequence alignments.

Starting from the results obtained from this structural and bioinformatics analysis, to evaluate in detail the possibility of the residues at positions 3, 7, and 12 to interact with thrombin ABE I hydrophobic cleft, the solvent-accessible surface area of these nucleotides was evaluated by calculating the Connolly surface with a probe radius of 1.4 Å, which approximates the radius of a water molecule (Viewer Module, Insight 2005, Accelrys Software Inc.). In particular, the Connolly surface of the considered nucleotides was calculated for the TBA experimentally determined structures (PDB IDs 1HAO, 1HAP, 4DIH, and 4DII) and for all conformers of TBA and new modified analogues, resulting from SA/MM calculations.

The TBA, TBA-$T_7$**b**, and TBA-$T_{12}$**b** SA/MM conformers presenting solvent-accessible surface areas of residues 3, 7, and 12 equal to or greater than that of the corresponding residue of TBA when interacting with the ABE I hydrophobic cleft in experimentally determined complexes (i.e., $T_3$, 191.01 Å$^2$; $T_7$, 159.35 Å$^2$; and $T_{12}$, 180.59 Å$^2$) were selected, and their occurrence rates were calculated. Because all experimental data refer to the mixture of the two diastereoisomers, the mean of the values obtained for the two diastereoisomers was also calculated.

Finally, with the aim to calculate the occurrence rates of bioactive conformations of residues at position 3, 7, and 12 of TBA and new modified analogues TBA-$T_7$**b** and TBA-$T_{12}$**b**, all conformers, resulting from SA/MM calculations, were superimposed on the experimentally determined structures of TBA in complex with thrombin (PDB IDs 1HAO, 1HAP, 1HUT, 4DIH, and 4DII) by fitting heavy atoms of the guanine bases of two quartets, and the overlap with the residue interacting with the ABE I hydrophobic cleft (I1e24, His71, I1e79, and Tyr117) was evaluated. To assess the bioactive conformation of the residue at position 7, the orientation that allows residue 7 to be located in the same position of $T_7$ of 1HAP or 1HUT crystal structure was considered (orientation II in Figure 2).

The conformation of residues at positions 3, 7, and 12 was considered bioactive when the correspondent nucleobase was positioned within the ABE I hydrophobic cleft and presented at least one atom superimposed on $T_3$ (PDB IDs 4DIH and 4DII) or on $T_7$ (PDB IDs 1HAP and 1HUT) or on $T_{12}$ (PDB ID 1HAO), respectively. Occurrence rates of bioactive conformations of residues at positions 3, 7, and 12 were then calculated. Because all experimental data refer to the mixture of the two diastereoisomers, the mean of the values obtained for the two diastereoisomers was also calculated.

## ■ ASSOCIATED CONTENT

### Ⓢ Supporting Information

Concentration-dependent response on PT value using increasing incubation times with human plasma; HPLC chromatograms; prolonged fibrinogen clotting time results in presence of human and bovine thrombin; calculated occurrence rates of *syn*, *anti*, and s/a conformers of TGT and TT glycosidic bonds; calculated occurrence rates of conformers presenting TGT and TT nucleobases "stacked" on the guanine planes; binding interactions between TBA and human thrombin ABE I in X-ray complexes; mutated amino acid residues in human and bovine thrombin ABE I; occurrence rates of SA/MM conformers presenting a solvent accessible surface area (Å$^2$) of residues 3, 7, and 12 equal to or greater than that of the corresponding residue of TBA assuming the bioactive conformation at ABE I hydrophobic cleft; occurrence rates of bioactive conformations at ABE I hydrophobic cleft of residues at position 3, 7, and 12, resulting from SA/MM calculations. This material is available free of charge via the Internet at http://pubs.acs.org.

## ■ AUTHOR INFORMATION

### Corresponding Author

*(M.V.) Phone: +39 081 678540. Fax: +39 081 678552. E-mail: varra@unina.it. (C.F.) Phone: +39 081 678544. Fax: +39 081 678552. E-mail: caterina.fattorusso@unina.it.

### Author Contributions

[§]These authors equally contributed to this work.

### Notes

The authors declare no competing financial interest.

## ■ ACKNOWLEDGMENTS

This work was supported by a PRIN grant 2009 from the Italian Ministero dell'Università e della Ricerca [2007EBYL8L_005] and a FARO grant 2012 from the University of Studies "Federico II". We thank Dr. Luisa Cuorvo for her valuable technical assistance.

## ■ ABBREVIATIONS USED

ON, oligonucleotide; TBA, thrombin-binding aptamer; ABE I, anion binding exosite I; SARs, structure−activity relationships; CD, circular dichroism; MM, molecular mechanics; MD, molecular dynamics; SA, simulated annealing; PT, prothrombin time

## REFERENCES


(1) (a) Huntington, J. A. Molecular recognition mechanisms of thrombin. *J. Thromb. Haemost.* **2005**, *3*, 1861−1872. (b) Di Cera, E. Thrombin interactions. *Chest* **2003**, *124*, 11S−17S.

(2) (a) Niu, W.; Chen, Z.; Gandhi, P. S.; Vogt, A. D.; Pozzi, N.; Pelc, L.; Zapata, F.; Di Cera, E. Crystallographic and kinetic evidence of allostery in a trypsin-like protease. *Biochemistry* **2011**, *50*, 6301−6307. (b) Gandhi, P. S.; Chen, Z.; Mathews, F. S.; Di Cera, E. Structural identification of the pathway of long-range communication in an allosteric enzyme. *Proc. Natl. Acad. Sci. U.S.A.* **2008**, *105*, 1832−1837. (c) Di Cera, E.; Page, M. J.; Bah, A.; Bush-Pelc, L. A.; Garvey, L. C. Thrombin allostery. *Phys. Chem. Chem. Phys.* **2007**, *9*, 1291−1306. (d) Di Cera, E. Thrombin as procoagulant and anticoagulant. *J. Thromb. Haemost.* **2007**, *5*, 196−202. (e) Lechtenberg, B. C.; Johnson, D. J. D.; Freund, S. M. V.; Huntington, J. A. NMR resonance assignments of thrombin reveal the conformational and dynamic effects of ligation. *Proc. Natl. Acad. Sci. U.S.A.* **2010**, *107*, 14087−14092.

(3) (a) Dahlback, B. Blood coagulation and its regulation by anticoagulant pathways: genetic pathogenesis of bleeding and thrombotic diseases. *J. Intern. Med.* **2005**, *257*, 209−223. (b) Desai, U. R. New antithrombin-based anticoagulants. *Med. Res. Rev.* **2004**, *24*, 151−181.

(4) Nimjee, S. M.; Oney, S.; Volovyk, Z.; Bompiani, K. M.; Long, S. B.; Hoffman, M.; Sullenger, B. A. Synergistic effect of aptamers that inhibit exosites 1 and 2 on thrombin. *RNA* **2009**, *15*, 2105−2111.

(5) (a) Bock, L. C.; Griffin, L. C.; Latham, J. A.; Vermaas, E. H.; Toole, J. J. Selection of single-stranded DNA molecules that bind and inhibit human thrombin. *Nature* **1992**, *355*, 564−566. (b) Li, W. X.; Kaplan, A. V.; Grant, G. W.; Toole, J. J.; Leung, L. L. A novel nucleotidebased thrombin inhibitor inhibits clot-bound thrombin and reduces arterial platelet thrombus formation. *Blood* **1994**, *83*, 677−682.

(6) (a) Schultze, P.; Macaya, R. F.; Feigon, J. Three-dimensional solution structure of the thrombin-binding DNA aptamer d(GGTTGGTGTGGTTGG). *J. Mol. Biol.* **1994**, *235*, 1532−1547. (b) Wang, K. Y.; Krawczyk, S. H.; Bischofberger, N.; Swaminathan, S.; Bolton, P. H. The tertiary structure of a DNA aptamer which binds to and inhibits thrombin determines activity. *Biochemistry* **1993**, *32*, 11285−11292. (c) Macaya, R.; Schultze, P.; Smith, F.; Roe, J.; Feigon, J. Thrombin-binding DNA aptamer forms a unimolecular quadruplex structure in solution. *Proc. Natl. Acad. Sci. U.S.A.* **1993**, *90*, 3745−3749.

(7) (a) Padmanabhan, K.; Padmanabhan, K. P.; Ferrara, J. D.; Sadler, J. E.; Tulinsky, A. The structure of α-thrombin inhibited by a 15-mer single-stranded DNA aptamer. *J. Biol. Chem.* **1993**, *268*, 17651−17654. (b) Padmanabhan, K.; Tulinsky, A. An ambiguous structure of a DNA 15-mer thrombin complex. *Acta Crystallogr. D: Biol. Crystallogr.* **1996**, *52*, 272−282. (c) Russo Krauss, I.; Merlino, A.; Randazzo, A.; Novellino, E.; Mazzarella, L.; Sica F. High-resolution structures of two complexes between thrombin and thrombin-binding aptamer shed light on the role of cations in the aptamer inhibitory activity. *Nucleic Acids Res.* **2012**, DOI: 10.1093/nar/gks512.

(8) Kelly, J. A.; Feigon, J.; Yeates, T. O. Reconciliation of the X-ray and NMR structures of the thrombin-binding aptamer d(GGTTGGTGTGGTTGG). *J. Mol. Biol.* **1996**, *256*, 417−422.

(9) Russo Krauss, I.; Merlino, A.; Giancola, C.; Randazzo, A.; Mazzarella, L.; Sica, F. Thrombin-aptamer recognition: a revealed ambiguity. *Nucleic Acids Res.* **2011**, *39*, 7858−7867.

(10) Pagano, B.; Martino, L.; Randazzo, A.; Giancola, C. Stability and binding properties of a modified thrombin binding aptamer. *Biophys. J.* **2008**, *94*, 562−569.

(11) Martino, L.; Virno, A.; Randazzo, A.; Virgilio, A.; Esposito, V.; Giancola, C.; Bucci, M.; Cirino, G.; Mayol, L. A new modified thrombin binding aptamer containing a 5′-5′ inversion of polarity site. *Nucleic Acids Res.* **2006**, *34*, 6653−6662.

(12) (a) Tasset, D. M.; Kubik, M. F.; Steiner, W. Oligonucleotide inhibitors of human thrombin that bind distinct epitopes. *J. Mol. Biol.* **1997**, *272*, 688−698. (b) Zhou, G.; Huang, X.; Qu, Y. Thi binding effect of aptamers on thrombin. *Biochem. Eng. J.* **2010**, *52*, 117−122.

(13) (a) Kim, Y.; Cao, Z.; Tan, W. Molecular assembly for high-performance bivalent nucleic acid inhibitor. *Proc. Natl. Acad. Sci. U.S.A.* **2008**, *105*, 5664−5669. (b) Müller, J.; Freitag, D.; Mayer, G.; Pötzsch, B. Anticoagulant characteristics of HD1-22, a bivalent aptamer that specifically inhibits thrombin and prothrombinase. *J. Thromb. Haemost.* **2008**, *6*, 2105−2112.

(14) Petrera, N. S.; Stafford, A. R.; Leslie, B. A.; Kretz, C. A.; Fredenburgh, J. C.; Weitz, J. I. Long range communication between exosites 1 and 2 modulates thrombin function. *J. Biol. Chem.* **2009**, *284*, 25620−25629.

(15) Sabo, T. M.; Farrell, D. H.; Maurer, M. C. Conformational analysis of γ′ peptide (410−427) interactions with thrombin anion binding exosite II. *Biochemistry* **2006**, *45*, 7434−7445.

(16) Tsiang, M.; Jain, A. K.; Dunn, K. E.; Rojas, M. E.; Leung, L. L.; Gibbs, C. S. Functional mapping of the surface residues of human thrombin. *J. Biol. Chem.* **1995**, *270*, 16854−16863.

(17) Schwienhorst, A. Direct thrombin inhibitors a survey of recent developments. *Cell. Mol. Life Sci.* **2006**, *63*, 2773−2791.

(18) (a) He, G.-X.; Krawczyk, S. H.; Swaminathan, S.; Shea, R. G.; Dougherty, J. P.; Terhorst, T. N2- and C8-substituted oligodeoxynucleotides with enhanced thrombin inhibitory activity in vitro and in vivo. *J. Med. Chem.* **1998**, *41*, 2234−2242. (b) Buff, M. C. R.; Schäfer, F.; Wulffen, B.; Müller, J.; Pötzsch, B.; Heckel, A.; Mayer, G. Dependence of aptamer activity on opposed terminal extensions: improvement of light-regulation efficiency. *Nucleic Acids Res.* **2010**, *38*, 2111−2118.

(19) (a) He, G.-X.; Williams, J. P.; Postich, M. J.; Swaminathan, S.; Shea, R. G.; Terhorst, T.; Law, V. S.; Mao, C. T.; Sueoka, C.; Coutré, S.; Bischofberger, N. In vitro and in vivo activities of oligodeoxynucleotide-based thrombin inhibitors containing neutral formacetal linkages. *J. Med. Chem.* **1998**, *41*, 4224−4231. (b) Saccá, B.; Lacroix, L.; Mergny, J.-L. The effect of chemical modifications on the thermal stability of different G-quadruplex-forming oligonucleotides. *Nucleic Acids Res.* **2005**, *33*, 1182−1192.

(20) (a) Oliviero, G.; Borbone, N.; Galeone, A.; Varra, M.; Piccialli, G.; Mayol, L. Synthesis and characterization of a bunchy oligonucleotide forming a monomolecular parallel quadruplex structure in solution. *Tetrahedron Lett.* **2004**, *45*, 4869−4872. (b) Oliviero, G.; Amato, J.; Borbone, N.; Galeone, A.; Petraccone, L.; Varra, M.; Piccialli, G.; Mayol, L. Synthesis and characterization of monomolecular DNA G-quadruplexes formed by tetra-end-linked oligonucleotides. *Bioconjugate Chem.* **2006**, *17*, 889−898. (c) Oliviero, G.; Amato, J.; Borbone, N.; D'Errico, S.; Galeone, A.; Mayol, L.; Haider, S.; Olubiyi, O.; Hoorelbeke, B.; Balzarini, J.; Piccialli, G. Tetra-end-linked oligonucleotides forming DNA G-quadruplexes: a new class of aptamers showing anti-HIV activity. *Chem. Commun.* **2010**, *46*, 8971−8973.

(21) Coppola, T.; Varra, M.; Oliviero, G.; Galeone, A.; D'Isa, G.; Mayol, L.; Morelli, E.; Bucci, M.-R.; Vellecco, V.; Cirino, G.; Borbone, N. Synthesis, structural studies and biological properties of new TBA analogues containing an acyclic nucleotide. *Bioorg. Med. Chem.* **2008**, *16*, 8244−8253.

(22) Pasternak, A.; Hernandez, F. J.; Rasmussen, L. M.; Vester, B.; Wengel, J. Improved thrombin binding aptamer by incorporation of a single unlocked nucleic acid monomer. *Nucleic Acids Res.* **2011**, *39*, 1155−1164.

(23) But, T. Y. S.; Toy, P. H. The Mitsunobu reaction: origin, mechanism, improvements, and applications. *Chem. Asian J.* **2007**, *2*, 1340−1355.

(24) (a) Lane, A. N.; Chaires, J. B.; Gray, R. D.; Trent, J. O. Stability and kinetics of G-quadruplex structures. *Nucleic Acids Res.* **2008**, *36*, 5482−5515. (b) Neidle, S.; Balasubramanian, S. The role of cations in determining quadruplex structure and stability. In *Quadruplex Nucleic Acids*; Neidle, S., Balasubramanian, S., Eds.; RCS Publishing: London, UK, 2006; pp 100−130. (c) Chaires, J. B.; Gray, R. D. Kinetics and mechanism of $K^+$- and $Na^+$-induced folding of models of human telomeric DNA into G-quadruplex structures. *Nucleic Acids Res.* **2008**, *36*, 4191−4209.

(25) (a) Jakubowski, H. V.; Kline, M. D.; Owen, W. G. The effect of bovine thrombomodulin on the specificity of bovine thrombin. *J. Biol. Chem.* **1986**, *261*, 3876−3882. (b) Liaw, P. C.; Fredenburgh, J. C.; Stafford, A. R.; Tulinsky, A.; Austin, R. C.; Weitz, J. I. Localization of the thrombin-binding domain on prothrombin fragment 2. *J. Biol. Chem.* **1998**, *273*, 8932−8939.
(26) Kretz, C. A.; Stafford, A. R.; Fredenburgh, J. C.; Weitz, J. I. HD1, a thrombin-directed aptamer, binds exosite 1 on prothrombin with high affinity and inhibits its activation by prothrombinase. *J. Biol. Chem.* **2006**, *281*, 37477−37485.
(27) Renault, J.; Laduree, D.; Robba, M. Synthesis and antiviral study of cyclopentano[d]pyrimidine-2,4-diones and octahydroquinazoline-2,4-diones acyclic nucleosides as potential anti-HIV agents. *Nucleosides, Nucleotides Nucleic Acids* **1994**, *13*, 891−901.
(28) Kibbe, W. A. OligoCalc: an online oligonucleotide properties calculator. *Nucleic Acids Res.* **2007**, *35* (Suppl. 2), W43−W46.
(29) (a) Hwang, T. L.; Shaka, A. J. Water suppression that works. Excitation sculpting using arbitrary wave forms and pulsed field gradients. *J. Magn. Reson. Ser. A* **1995**, *A112*, 275. (b) Dalvit, C. Efficient multiple-solvent suppression for the study of the interactions of organic solvents with biomolecules. *J. Biomol. NMR* **1998**, *11*, 437.
(30) Dauber-Osguthorpe, P.; Roberts, V. A.; Osguthorpe, D. J.; Wolff, J.; Genest, M.; Hagler, A. T. Structure and energetics of ligand binding to proteins: *E. coli* dihydrofolate reductase-trimethoprim, a drug receptor system. *Proteins* **1988**, *4*, 31−47.
(31) Fletcher, R. Unconstrained optimization. In *Practical Methods of Optimization*; Wiley: New York, 1980; Vol. *1*.
(32) (a) Neidle, S. *Principles of Nucleic Acid Structures*; Academic Press: London, UK, 2008. (b) Reichert, J.; Sühnel, J. The IMB Jena Image Library of Biological Macromolecules 2002 Update. *Nucleic Acids Res.* **2002**, *30*, 253−254.